Lower nappe aeration in smooth channels: experimental data and numerical simulation

EUDES J. ARANTES[1], RODRIGO M. PORTO[2], JOHN S. GULLIVER[3],
ALBERTO C.M. LIMA[4] and HARRY E. SCHULZ[2,5]

[1]UTFPR, Campus Campo Mourão, Caixa Postal 271, 87301-005 Campo Mourão, PR, Brasil
[2]Departamento de Hidráulica e Saneamento/EESC/USP,
Av. Trabalhador São-carlense, 400, 13566-590 São Carlos, SP, Brasil
[3]Department of Civil Engineering, University of Minnesota, 2 Third Avenue S.E, 55455 Minneapolis, MN, USA
[4]Universidade da Amazônia, Av. Alcindo Cancela, 287, Umarizal, 66060-000 Belém, PA, Brasil
[5]Núcleo de Engenharia Térmica e Fluidos/EESC/USP,
Av. Trabalhador São-carlense, 400, 13566-590 São Carlos, SP, Brasil

ABSTRACT

Bed aerators designed to increase air void ratio are used to prevent cavitation and related damages
spillways. Air entrained in spillway discharges also increases the dissolved oxygen concentration of th
water, which can be important for the downstream fishery. This study considers results from a systemat
series of measurements along the jet formed by a bed aerator, involving concentration profiles, pressu
profiles, velocity fields and corresponding air discharges. The experimental results are, then, compare
with results of computational fluid dynamics (CFD) simulations with the aim of predicting the air dischar
numerically. Comparisons with jet lengths and the air entrainment coefficients from the literature are al
made. It is shown that numerical predictive tools furnish air discharges comparable to measured value
However, if more detailed predictions are desired, verification experiments are still necessary.

Key words: spillway aerators, air entrainment, air-water flows, multiphase flows.

INTRODUCTION

Bottom aerators are a technique used to prevent cavitation erosion on spillways and to enhance the c
content of the water. Air vented through the bottom aerators is entrained into the flowing water, incr
the compressibility of the air-water mixture and lowering the velocity of pressure waves. When imp
of cavitation bubbles occurs, the higher compressibility of the surrounding fluid dampens the impact
pressure waves. Additionally, the bubbles increase the contact area between air and water, improvi

Experimental investigations on spillway air entrainment by bottom aerators have resulted in empirical design equations. Schwarz and Nutt (1963) presented a theoretical equation for the jet length formed after the ramp. Pan et al. (1980) and Pinto et al. (1982) related the air discharge to geometrical parameters of the jet. Additionally, Tan (1984) and Rutschmann and Hager (1990) explained the dependence of the air discharge on the jet length. The jet length predictions obtained by Tan (1984) are close to those of Schwarz and Nutt (1963).

In Brazil, the studies on aerated spillways were intensified during the construction of the hydropower dams in the 1970 and 1980 decades. The first relevant conclusions for spillways were presented by Pinto et al. (1982), while Borsari (1986) and Fuentes (1992) furnished reviews of important studies and procedures. These aerator studies helped in the establishment of locally adopted procedures. Some early studies, like Volkart (1980) and Wood (1985), added important conceptual contributions for the understanding of aerated flows. Practical applications of the research results, however, require more detailed measurements and the review of existent results. Kökpinar and Gögüs (2002) conducted an extensive experimental study and furnished correlations not only for the jet length, but also for the air entrainment in lower and upper nappes, and a graphical presentation of the effect of ramp heights and bed slopes. The redistribution of flow velocity in the aeration zone was considered by Toombes and Chanson (2005), while the details of the geometry of the air-water interface were used to propose the concept of "entrapped air" by Wilhelms and Gulliver (2005). A similar entrapped air concept was used by Lima et al. (2008) to explain measurements of air void ratios in lower nappe aeration.

This paper seeks to compare CFD simulations with a detailed experimental study of the lower nappe of a jet generated by an aerator in a laboratory chute. Measurements of velocity fields, pressure and air concentration (void ratio) profiles will be compared to CFD results. The CFD simulations of air discharges were comparable to the measured values. It is also shown that, if a more detailed description is needed, experiments are still necessary.

EXPERIMENTAL METHODS

The experiments were conduced in a chute built in the Laboratory of Environmental Hydraulics of the School of Engineering at São Carlos, Brazil. The chute had a slope of 14.5°, an useful length of 5.0 m, with a rectangular cross section 0.20 m wide and 0.50 m high. The bed aerator was composed of a ramp with a length of 23.0 cm, a final height $t_r = 4.0$ cm and an angle of 10° relative to the chute. The chamber under the jet had a depth of 12.0 cm, a length of 18.0 cm and a width of 20.0cm. The air discharge was measured in the air supply tube, which had a diameter of 71.65mm. Air velocities were obtained from pressure measurements, with a micromanometer having one side opened to the atmosphere and the other fixed in a pre-calibrated position in the tube. The concentration measurements in the flow were made with a Cesium 137 probe, as shown in Figure 1. Calibration was made with the channel *a)* full with water and *b)* empty. The Cesium 137 radiation was projected perpendicularly to the flow in the channel and a counter registered the remaining radiation after passing the mixture of air and water and the glass walls. The concentration

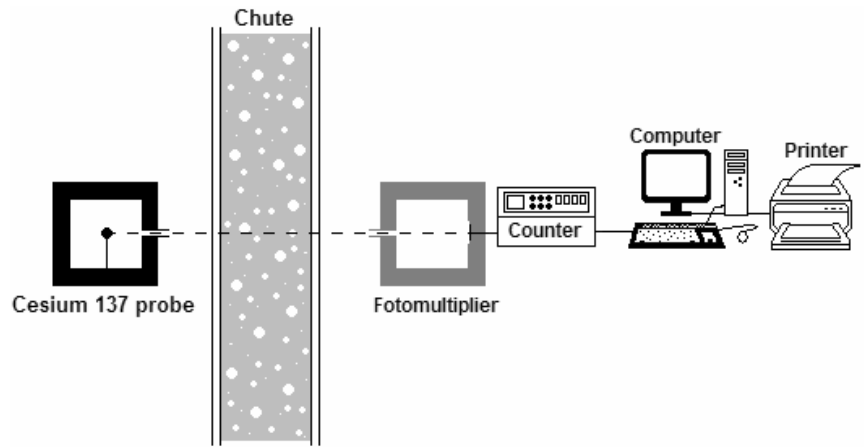BED AERATION IN SMOOTH CHANNELS: EXPERIMENTS AND NUMERICAL SIMULATION

Fig. 1 – Equipment used for the concentration measurements with Cesium 137 probe.

An electromagnetic flow meter was used to measure the water discharges, which were checke[d]
a rectangular weir located at the outlet of the channel. The measurement of velocity fields in the j[et]
performed for nine runs, using a mirror inside of the flow. Velocity fields were measured using p[article]
image velocimetry (PIV). The light source was a copper gas Laser, with a mean power of 20 W and [pulsing]
at 10 kHz. The pulse power ranged from 60 to 140 kW. Generated wavelengths were 510.6 nm ([green)]
and 578.2 nm (yellow). A CCD camera with a resolution of 1024 pixels × 1024 pixels was used to [capture]
the images. After capturing and storing the images in the computer, PIV software was applied t[o each]
image to obtain velocity vector fields by using auto-correlation calculations. 234 images were tak[en for]
each run. Figure 2 shows all cross sections used in the present study. Sections 1, 2 and 3 were u[sed to]
obtain the approach flow information (velocity and water depth). Sections 4 through 8 were used [for]
concentration measurements. Additional sections S_{IX} and S_X were used for velocity measurements [in the]
jet core. For velocity measurements in sections 1 and 2, the laser sheet was introduced in the flow fr[om the]
bottom of the channel.
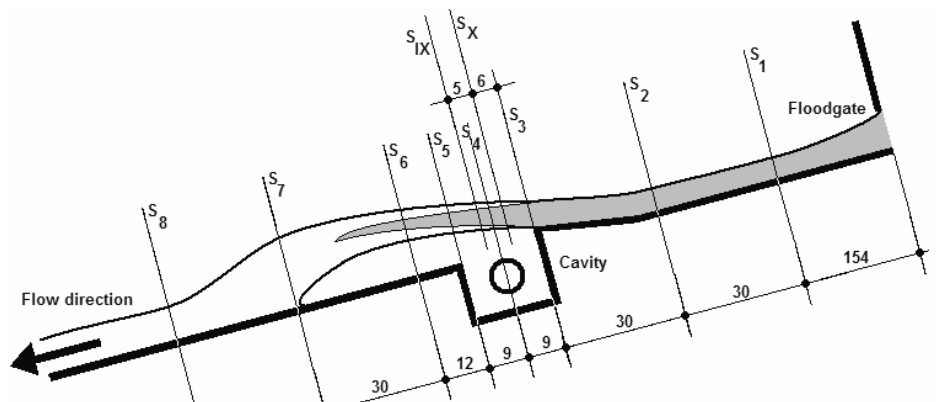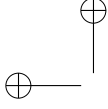
For velocity measurements in the jet core, a mirror was positioned downstream in the jet before the upper and lower white water regions came together, as shown in Figure 3, and the laser sheet was introduced into the flow from the side of the channel. Detailed descriptions of the chute and the measurement equipment may be found in Carvalho (1997) and Lima (2004).
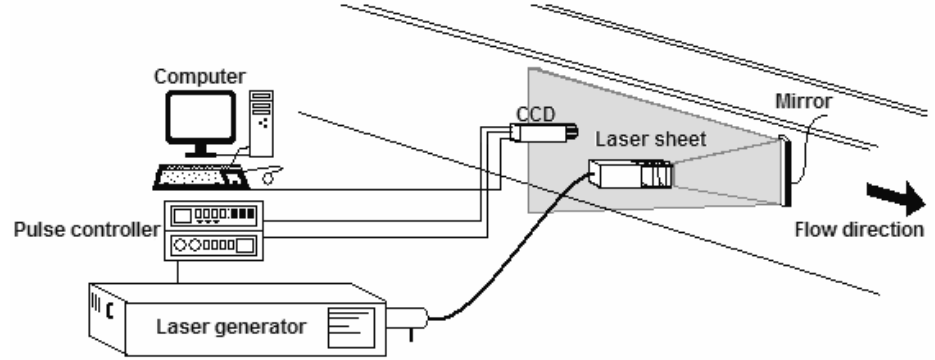
Fig. 3 – Experimental arrangement for the velocity measurements in the jet core using a mirror.

SIMULATION METHODS

In this study, the inhomogeneous multiphase model was applied with the liquid and the gaseous phases considered. There is one solution field for each separate phase, and the fluids interact via interphase transfer terms. For example, the two phases may have separated velocity and temperature fields, but there will be a tendency for these to come to an equilibrium through interphase drag and heat transfer terms (CFX 2004).

The following equations for inhomogeneous multiphase flow were used to simulate the air and water flows, and air uptake:

Continuity Equations:

$$\frac{\partial}{\partial t}(r_a \rho_a) + \nabla \times (r_a \rho_a \cup_a) = S_{MSa} + \sum_{b=1}^{N_p} \Gamma_{ab} \tag{1}$$

Momentum Equations:

$$\frac{\partial}{\partial t}(r_a \rho_a \cup_a) + \nabla \times (r_a(\rho_a \cup_a \times \cup_a)) =$$

$$-r_a \nabla p_a + \nabla \times (r_a \mu_a(\nabla \cup_a + (\nabla \cup_a)^T)) + \sum_{b-1}^{N_p} (\Gamma_{ab}^+ \cup_b - \Gamma_{ba}^+ \cup_a) + S_{MA} + M_a \tag{2}$$

where: r_a is the volume fraction of each phase (phases indicated by "a", with "a" assuming values from 1 to N_p, the total number of phases), ρ_a is the density of phase "a", $\overrightarrow{U}_a$ is the velocity vector of phase "a", μ_a is the viscosity of phase "a", S_{MSa} represents mass sources specified by the user; Γ_{ab} is the mass
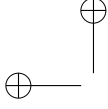
momentum transfer induced by interphase mass transfer. The volume fractions of the phases sum to
that is:

$$\sum_{a=1}^{N_p} r_a = 1$$

There are $4N_P + 1$ equations to describe the fluid dynamics for the $5N_P$ unknowns r_a, $U_a||$, $||V$
(components of the velocity vectorial field $\overrightarrow{U}_a$), and P_a (the pressure field of each phase). The add
$N_P - 1$ equations needed to close the system of equations were supplied by assuming that all
shared the same pressure field, P, that is:

$$P_a = P \quad \text{for all} \quad a = 1, \ldots, N_P$$

A scalar variable ϕ in phase "a" has the corresponding transport equation:

$$\frac{\partial}{\partial t}\left(r_a \rho_a \phi_a\right) + \nabla \times \left(r_a \left(\rho_a \cup_a \phi_a\right)\right) - \nabla \times \left(r_a \left(\rho_a D_a^{(\phi)} + \frac{\mu_{ta}}{Sc_{ta}}\right)\nabla \phi_a\right) = S_a^{(\phi)} + T_a^{(\phi)}$$

where $D_a^{(\phi)}$ is the Diffusivity of ϕ_a, $S_a^{(\phi)}$ represents an external source in phase "a", and $T_a^{(\phi)}$ repr
sources of ϕ_a due to interphase transfers. Details of the multiphase model may be found in CFX (20

To initialize a simulation, a relatively gross mesh was first used to locate the air-water interface.
the regions of the upper and lower free surfaces were refined, allowing a detailed location of the int
for the definitive run. The final mesh of each case presented a higher concentration of cells in the
and lower nappes of the jet, as shown in Figure 4. Details are described by Arantes (2007). Table I
the main characteristics of the grids and the simulated fluids (air and water). The number of nod
elements of the grids are mean values for all simulated conditions.

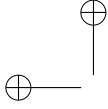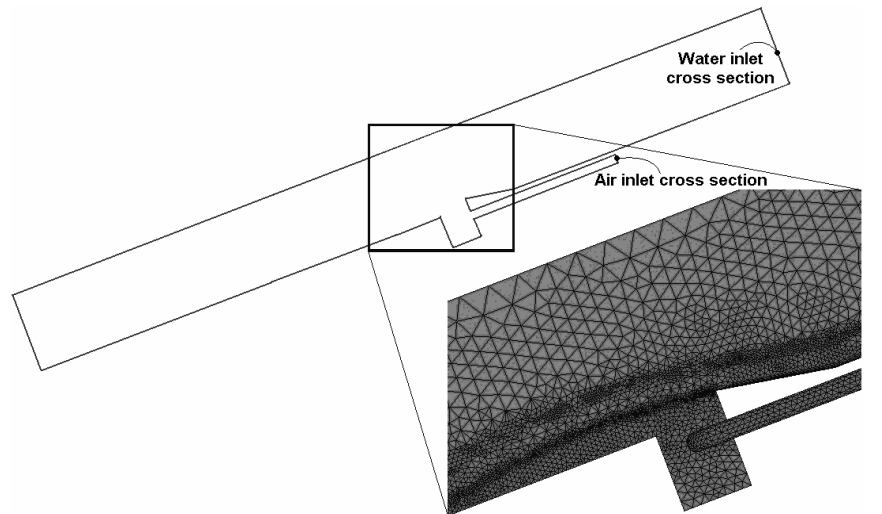Fig. 4 – Example of refined mesh used for the numerical calculations.

TABLE I
The Domain, Fluids and Simulation characteristics, initial and boundary conditions.

Domain (after adaptation)	
Number of Nodes	≈ 550000
Number of Elements	≈ 2750000
Fluid: Water	
Temperature	25°C
Dynamic Viscosity	$8.899*10^{-4}$ kg.m^{-1}.s^{-1}
Density	998 kg.m^{-3}
Surface Tension Coef.	0.0732 N.m^{-1}
Fluid: Air	
Temperature	25°C
Dynamic Viscosity	$1.831*10^{-5}$ kg.m^{-1}.s^{-1}
Density	1.185 kg.m^{-3}
Simulation	
Time step	0.1 s
Simulation Time	10 s
Processor Characteristics	Processor 3.2 GHz (Opteron 64 bits)
CPU Processing time	$\approx 1*10^5$ s

a portion of the observed results. The CFX standard constants and conditions, on the other hand, led to acceptable predictions for the whole set of experiments, being thus used in this study.

The conditions in the inlet were imposed as:

– Pressure: hydrostatic pressure,

– Turbulence intensity: fixed at 5% of the water velocity (standard for CFX),

– Turbulence model: SSG Reynolds Stresses using CFX standard parameters. The model allows the simulation of non-isotropic situations, and the use of the law of the wall.

– Roughness for the law of the wall: 1.0 mm.

The calibration was primarily based on the predictions of the jet lengths.

RESULTS AND DISCUSSION

Fourteen runs were conducted in the chute. Table II provides the experimental conditions. The jet length of run 2 is not available because the jet was longer than the channel. Velocity field measurements using
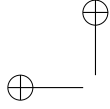
BED AERATION IN SMOOTH CHANNELS: EXPERIMENTS AND NUMERICAL SIMULATION

TABLE II
Experimental conditions.

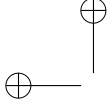| Run	Opening of the floodgate H (cm)	Depth at S2 h (cm)	Water flow rate Q_w (l/s)	Velocity at S2 V_w (m/s)	Froude Number Fr	Jet Length L (m)	Air flow rate Q_{air} (l/s)	Air Temp. (°C)	Water Temp. (°C)
1*	3	3.37	45.77	6.79	11.81	2.08	23.06	27.5	24.2
2*		3.51	63.93	9.11	15.52	NA	27.82	26.0	25.1
3*	6	5.26	47.65	4.53	6.31	1.08	12.66	24.0	22.0
4		5.50	58.85	5.35	7.28	1.38	18.37	24.7	24.0
5*		5.40	64.37	5.96	8.19	1.48	20.17	25.5	24.1
6*		5.85	92.05	7.87	10.39	2.28	29.49	23.0	24.1
7	9	6.00	44.44	3.70	4.82	0.78	9.92	29.0	28.0
8*		7.05	64.38	4.57	5.50	0.98	14.26	28.0	22.5
9*		8.31	98.20	5.91	6.55	1.48	22.92	21.4	21.0
10		8.54	119.86	7.02	7.67	2.08	31.69	29.0	22.0
11	11	6.92	46.58	3.37	4.09	0.68	11.28	23.8	21.8
12*		7.94	64.38	4.05	4.59	0.88	15.52	25.8	23.0
13*		9.10	94.64	5.20	5.50	1.18	20.28	25.8	22.1
14		10.16	128.76	6.34	6.35	1.58	27.45	21.4	21.0

COMPARISON OF MEASUREMENTS WITH LITERATURE

Verification of the jet length L

Jet lengths are commonly used to quantify the air uptake by the water flows. The jet lengths of T
were compared with theoretical predictions of Schwarz and Nutt (1963) and Tan (1984), given respec
by equations 6 and 7, and plotted in Figure 5. Also shown are the predictions of the empirical corre
of Kökpinar and Gögüs (2002), given by equation 8. The theoretical equations 6 and 7 were obtaine
no restrictions to α. Equation 8 was adjusted from experimental data, being thus restricted by the ra
α tested during the experiments. A systematic underestimation of equation 8 is observed, which n
due to extrapolations of its limits of application. For example, the ramp slope is limited to $0 < \alpha <$
but in this study $\alpha = 10°$.

The good agreement between measured and literature results is taken as an indication that the e
mental data for jet length can be used to compare with CFD simulations.

$$\frac{L}{h} = \frac{\overline{\alpha}(1 + \overline{\alpha}\tan\theta)}{\cos\theta} Fr^2 \left\{ 1 + \left[1 + 2\frac{t_r + t_s}{h} \frac{\cos\theta}{(\overline{\alpha}Fr)^2} \right] \right\} + \frac{t_r + t_s}{h}\tan\theta$$

$$\frac{L}{h} = 0.28(1 + \alpha)^{0.22} \, Fr^{1.75} \left(\frac{t_r + t_s}{h}\right)^{0.44} \left[(1 + \tan\theta)\frac{A_a}{A_w}\right]^{-0.087} \tag{8}$$

In the above equations, α is the ramp slope, θ is the chute slope, $\overline{\alpha}$ is the take off angle (which is the angle followed by the liquid when it leaves the ramp). $\overline{\alpha}$ is equal to α because no inertial effects altered the observed direction of the flow after leaving the ramp), t_r is the ramp height, t_s is the step height (zero in the present experiments), t is the time, ρ_w is the water density, g is the gravity acceleration, ΔP is the relative pressure under the jet (taken positive), h, V, Fr and L are defined in Table I, and A_{air}/A_w is the ratio between the air supply pipe entrance area, A_a, and the area of the water flow before the aerator, A_w.
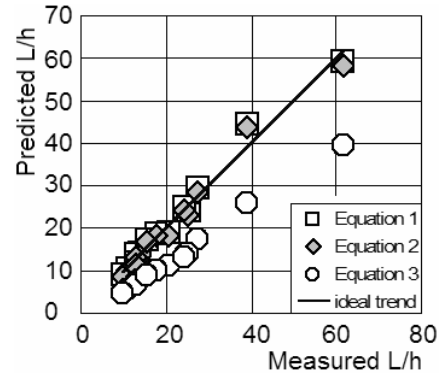

Fig. 5 – Predicted and measured jet lengths.

Verification of the air entrainment coefficient β as a function of L/h

Pinto et al. (1992) proposed that the ratio between Q_{air} and $Q_w||$, $||Q_{air}/Q_w$, is proportional do L/h, with a coefficient of proportionality between 0.023 and 0.033. Rutschmann and Hager (1990) found a coefficient of proportionality of 0.030, for the maximum value of β (zero relative pressure in the cavity under the jump). The authors showed that the straight line of β *vs.* L/h intercepted the L/h axis around $L/h = 5$ for a first set of data, so that the equation $\beta = 0.030(L/h - 5)$ was proposed. For a second set of data, the simple proportionality $\beta = 0.030L/h$ was followed. The authors measured L/h up to around 45. Chanson (1991) suggested that β and L/h follow linear trends with lower slopes for $L/h < 20$ and higher slopes for $L/h > 20$. The L/h values ranged up to around 25. Kökpinar and Gögüs (2002) presented the empirical correlation

$$\beta = 0.0189(L/h)^{0.82}\big[(A_a/A_2)(1 + \tan\theta)\big]^{0.24} \tag{9}$$

in which the coefficient of $\beta = \beta(L/h)$ depends on the channel slope (θ) and the ratio A_{air}/A_w. L/h ranged up to 30. Equation 9 shows a nonlinear dependence between β and L/h, and that the coefficient may be lower than 0.0189. The equation is valid for $0 < \theta < 51.3°$.

Figure 6 shows β against L/h for the data of these experiments. A constant β seems to occur for L/h
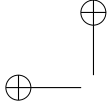
BED AERATION IN SMOOTH CHANNELS: EXPERIMENTS AND NUMERICAL SIMULATION

and Hager (1990), for $\theta = 51.3°$ and $\theta = 34.4°$. The dependence of the function $\beta = \beta(L/$
geometrical characteristics, such as the slope of the spillway, is clearly visible. Applying equation 9
conditions of this study ($\theta = 14, 5°$) led to good predictions of the measured data, with deviations occ
for the lower range of L/h. These deviations may be due to the extrapolations of the application li
equation 9 or bias in the measurements. As already mentioned, the used ramp slope $\alpha = 10°$ extrap
the $0 < \alpha < 9.45°$ limits. Also the experimental range of Froude numbers (Fr), $4.08 < Fr <$
extrapolates the application limits of equation 4, given as $5.56 < Fr < 10.00$. However, equation 9
that the data followed the general expected behavior for the applied experimental conditions, indicati
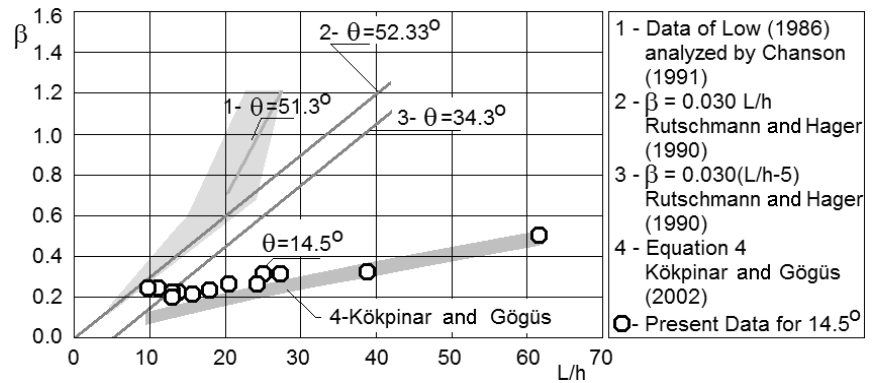the experimental data for air/water flow ratio can be used to compare with CFD simulations.

Fig. 6 – Measured β and L/h values, together with data and correlations from other authors. θ is the angle of the spillway
experiment. The present set of data approximates to the general trend of the correlation of Kökpinar and Gögüs (2002).

Verification of the air entrainment coefficient β as a function of Fr

Figure 7 shows the β data of the present study (white circles) and those of Kökpinar and Gögüs
(gray circles) against the Froude number. The data of Kökpinar and Gögüs were obtained for flows
step height ts of 5 cm, while, for the present data, $t_s = 0$. Moreover, their t_r/h values ranged from
0.4, while in the present study they ranged from 0.4 to 1.2. The different experimental conditions gen
clouds of points with similar trends, but separated in the graph β *vs. Fr*, as shown in Figure 7.
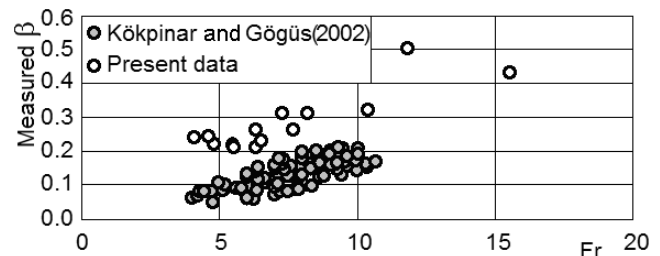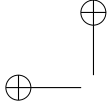

Fig. 7 – Measured β against the Froude number.

The combined effect of t_r and t_s is represented here through the ratio $(t_r + k \cdot t_s)/h$, where k is an adjusted constant. A multiple regression analysis furnished the result

$$\beta = 0.0278 \, Fr^{1.044} \left(\frac{t_r + 3t_s}{h} \right)^{-0.460} \tag{11}$$

Predicted and measured data are presented in Figure 8, showing that the present data and those from literature are complementary and form a single cloud of points. The agreement between present and literature data (Figs. 5, 6 and 8) allowed the use of the corresponding experimental results of air concentration profiles, pressure profiles, velocity profiles and air discharges to compare to the CFD predictions.
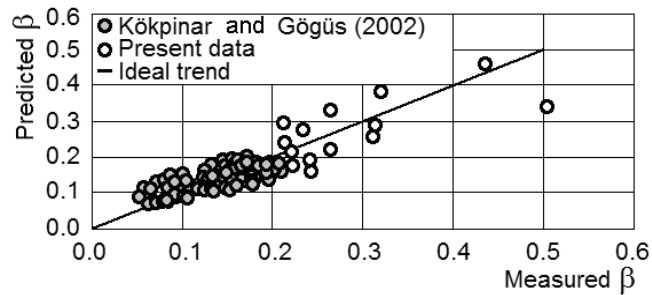

Fig. 8 – Calculated β obtained using equation 6 against measured β.

COMPARISON OF CFD PREDICTIONS WITH EXPERIMENTS

Jet length

Table III shows six predictions of the jet length. As mentioned, the turbulence conditions were adjusted in the inlet of the numerical domain, but the CFX standard parameters of the turbulence model furnished the best predictions for the set of jet lengths. These conditions were similar for all runs. The simulated lengths were in the range of 0.81 to 1.08 times the measured length for the six runs. These runs were used to obtain numerical air discharges.

TABLE III
Simulated runs, showing predicted and measured
lengths of the jet.

Run	Measured Length (m)	Predicted Length (m)	$\dfrac{L_{predicted}}{L_{measured}}$
3	1.08	1.17	1.08
5	1.48	1.18	0.81
8	0.98	1.02	1.04
9	1.48	1.32	0.89
12	0.88	0.88	1.00

BED AERATION IN SMOOTH CHANNELS: EXPERIMENTS AND NUMERICAL SIMULATION

Pressure distribution

The pressure distribution along the channel bed was used to measure the jet length, taken as the posi[...]
the pressure peak. Figure 9 presents an example measurement and simulation results for run 13, sh[...]
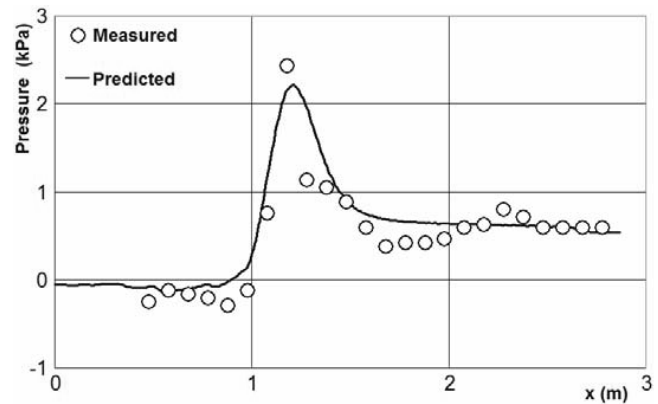good agreement between CFD simulations and the experiment.

Fig. 9 – Pressure distribution along the channel bed for run 13. The axis *x*
represents the longitudinal distance with origin taken at the beginning of the jet.

Velocity distribution

The velocity distribution in section S3, measured using the PIV technique, was compared with the pre[...]
distribution. Figure 10 shows the comparison for runs 3 and 5, taken as examples. The agreement be[...]
measured and predicted profiles is considered acceptable, having a maximum difference of ten percen[...]
imposed turbulence intensity in the inlet of the numerical domain, maintained constant for all simul[...]
may be a cause of the observed deviations. No numerical bias of the related concentration field[...]
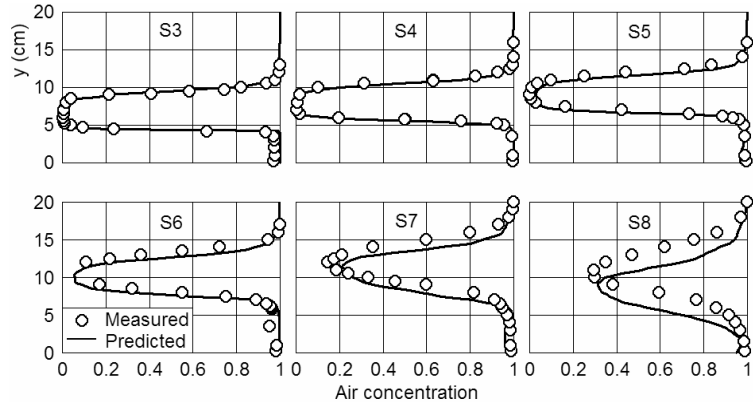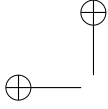observed (see Fig. 11), so that the obtained velocity distributions were considered adequate for this[...]
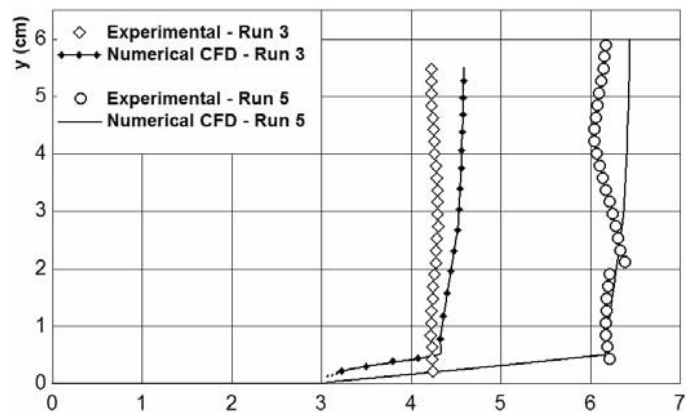
Fig. 11 – Void ratio profiles along the jet upstream of the reattachment section (run 5).

Concentration profiles

Lima et al. (2008) presented measured values for the air discharge entering into the cavity under the jet, and also values obtained calculating the air discharge from air concentration profiles measured at cross sections along the lower nappe of the jet. The authors applied Equation (12) along sections 4 through 8 (Fig. 2), corresponding to a distance between 3.9% and 132% of the jet lengths.

$$Q_x = B \int_{\text{Lower boundary}}^{\text{Upper boundary}} C(y)V_x(y)dy \tag{12}$$

where Q_x is the air discharge, B is the channel width, C is the air concentration (void ratio), V_x is the velocity in the x direction and y is the distance normal to the chute face. The upper and lower boundaries of the domain were set at two conditions: 1) C values of 95% and 5%, and 2) C values of 90% and 10%.

Lima et al. (2008) showed that the measured air discharges are substantially lower than the air discharges evaluated from the concentration profiles. Previous results of Wilhelms and Gulliver (2005), when evaluating entrained air from concentration profiles for upper surface aeration, showed that corrections must be made because the measurements involve air among water parcels of the surface distortions, not absorbed by the water. Lima et al. (2008) suggested that a similar effect influenced the measurements along the lower nappe, with the addition of the effect of the spray that emanates from the aerator lip as water. Substantial sprays could account for water measurement throughout the air pocket, affecting the air discharge results.

Numerical predictions of air concentrations are shown in Figure 11. Run 5 is presented because it represents the worst agreement between the measured and predicted jet lengths (predicted length = 81% of measured length). Even for this condition, the agreement between measured and predicted concentration profiles is good. The displacement observed between profiles, mainly for sections S7 and S8, is due to the lower predicted position of the jet when compared with the measured position.
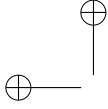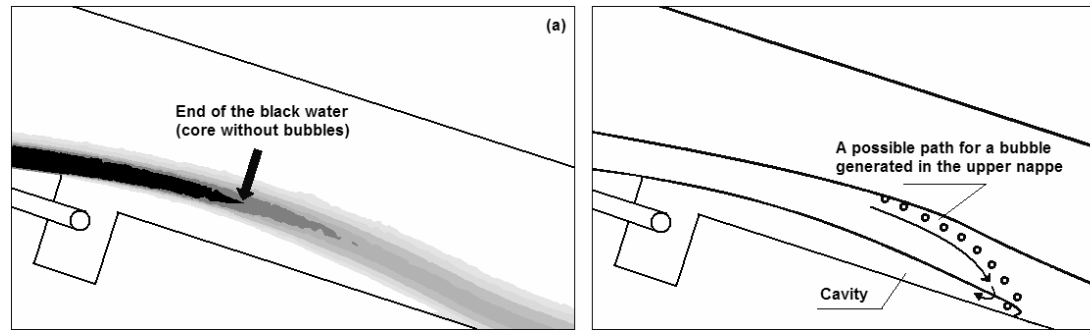
Fig. 12 – a) Concentration field along the jet, showing the end of the region of the water core with zero air concentration (
b) A sketch of a possible path followed by a bubble originated in the upper nappe.

profiles of the upper and lower nappes interact downstream of the position indicated by the black
in Figure 12a, where the concentration in the water core ceases to be zero (shown in black). Non-z
concentrations in the core are related to bubbles originating either at the upper or at the lower su
Figure 12b shows a sketch of an eventual intrusion of air originated in the upper nappe. In thi
concentration measurements can also be affected by this new air source, and air discharges obtaine
concentration measurements can eventually be different from those measured in the inlet structure.

The measured and calculated concentration profiles for the impact region could also be compa
one run of the present set of experiments. Figure 13 shows the results obtained for run 12 at section
only case in which the pressure point that quantifies the jet length coincided with a measurement s
Although the general behavior of both profiles is the same, substantial differences are observed be
the concentration values. The measured profile is, in general, steeper than the calculated profile, a
concentration differences are higher for distances to the channel bottom between 0 and 5 cm. A
this case, the differences may result from the turbulence condition imposed in the inlet of the simu
domain. For example, higher levels of homogenization (softer profiles) are obtained for higher tu
diffusivities, which are dependent on the turbulent conditions.
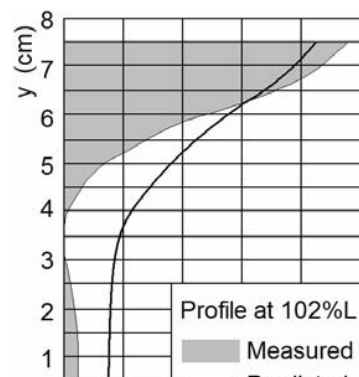
Air discharges

Predicted air discharges are compared with measurements for the six simulated cases presented in Figure 14. Although the predicted air discharges have the same magnitude as the measured air discharges, a relatively high spread is observed. The predicted air discharges were obtained by integrating air concentration at the cross section of the inlet tube (Fig. 2). The differences between experimental and numerical data are probably associated with the constant parameters of the turbulence model (the CFX standards were used) for the different experimental situations, and the constant turbulence intensity in the inlet of the numerical domain (5%), as previously mentioned. As shown by Ervine et al. (1995), the air uptake by the water depends on the turbulence intensity perpendicular to the flow direction.
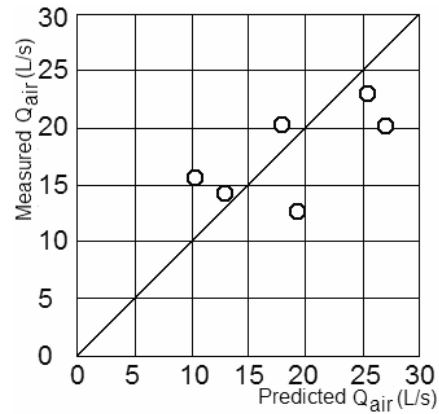

Fig. 14 – Comparison between measured and predicted air discharges, for the six conditions simulated in the present study.

The results indicate that, for a first evaluation of the magnitude of the air discharge, numerical procedures can be used to help in the decision-making process. However, the numerical code must be calibrated, based on measured characteristics. In the present study, the jet lengths were used to calibrate the model (to adjust parameters and inlet conditions), and the measured concentration, pressure, and velocity profiles were used to check the numerical results. If more detailed information is needed, say for cavitation erosion potential, it is still necessary to conduct experimental studies and to scale up the results based on empirical procedures.

CONCLUSIONS

Experimental studies on air absorption by flows over a bed aerator were described and compared with theoretical and empirical predictions found in the literature and computational results conducted here.

1. Jet lengths were well predicted by the equations of Schwarz and Nutt (1963) and Tan (1984). The air entrainment coefficients β, when expressed as a function of L/h, were well predicted by the equation of Kökpinar and Gögüs (2002), unless for the lower range of L/h, that is, for $\sim 10 < L/h < \sim 15$.
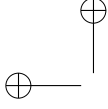
BED AERATION IN SMOOTH CHANNELS: EXPERIMENTS AND NUMERICAL SIMULATION

data here described and those of Kökpinar and Gögüs (2002) can be presented together, foll
the same trend.

2. Computational predictions of the jet length were taken as control parameter for the numerica
   ulations (calibrations). The CFX standard parameters were adopted for the turbulence mode
   turbulence intensity at the inlet was fixed at 5% of the mean flow velocity, and the roughness u
   the law of the wall was fixed at 1.0 mm, which generated predicted jet lengths between 0.8 a
   times the measured length.

3. It was observed that the pressure distribution along the channel bed, the velocity profiles at the end
   ramp, and the concentration profiles along the jet could be represented by the calibrated computa
   code. Considering the air concentration at the impact point, the measured and predicted p
   presented the same general form, although concentration differences were observed.

4. The computational predictions of the air discharges followed the magnitude of the measured
   However, a relatively large scatter was observed. For a first evaluation of the magnitude of
   discharge, computational procedures can be used to help in making decisions. However, the num
   code must be calibrated, based on previous measured characteristics. In the present study,
   lengths were used to calibrate the model (to adjust parameters and inlet conditions), and the me
   concentration, pressure, and velocity profiles were used to check the numerical results.

NOMENCLATURE TABLE

a	a physical phase	t	time
A	amplitude of oscillation	t_r	ramp height
A_a	area crossed by air	t_s	step height
A_w	area crossed by water	$T_a^{(\phi)}$	sources of ϕ_a
B	channel width	$\overrightarrow{U}_a$	velocity vector of phase a
C	air concentration (void ratio)	U_a, V_a, W_a	components of $\overrightarrow{U}_a$
$D_a^{(\phi)}$	diffusivity of ϕ_a	V	generic velocity
Fr	Froude number	V_x	velocity in the x direction
g	acceleration of gravity	x	longitudinal axis
h	height	y	distance normal to the chute face
L	jet length	α	ramp slope
M_a	interfacial forces acting on phase a	$\overline{\alpha}$	take off angle
N_p	total number of physical phases	β	air entrainment coefficients ($\beta = Q_a/Q$
P_a	pressure field of phase a	Γ_{ab}	specific mass flow rate from phase b to a
Q_a	air discharge	ϕ_a	conserved specific variable of phase a
Q_w	water discharge	ΔP	relative pressure under the jet
r_a	volume fraction of phase a	μ_a	viscosity of phase a
$S_a^{(\phi)}$	external source in phase a	θ	chute slope
S_{Ma}	momentum sources	ρ_a	density of phase a

536 EUDES J. ARANTES et al.

RESUMO

Aeradores de fundo projetados para aumentar a concentração de ar são utilizados para previnir a cavitação e danos dela derivados em vertedouros. O oxigênio contido na água também é um parâmetro relevante para garantir alta qualidade das águas a jusante do vertedouro, com reflexos na qualidade ambiental. Equações e critérios de projeto existentes ainda são considerados aproximados, mostrando a necessidade de mais estudos para elucidar os mecanismos que governam o carreamento de ar. Este trabalho apresenta resultados de uma série sistemática de medidas de concentração de ar ao longo da superfície inferior do jato de um aerador de fundo, juntamente com medidas pertinentes de descargas de ar e campos de velocidade da água. Foram feitas comparações com resultados da literatura, considerando perfis de concentração ao longo do jato do aerador até a região de jusante. As medições sob condições controladas forneceram informações necessárias para testar resultados numéricos de aeração obtidos em simulações desses escoamentos, utilizando mecânica dos fluidos computacional (CFD). Mostra-se que ferramentas numéricas preditivas fornecem vazões de ar comparáveis aos valores medidos. Também é concluído que, se detalhes são necessários, experimentos são ainda úteis.

Palavras-chave: aeradores de vertedouros, carreamento de ar, escoamento ar-água, escoamentos multifásicos.

REFERENCES

ARANTES EJ. 2007. Caracterização do Escoamento sobre Vertedores em Degraus via CFD. Tese de Doutorado, Escola de Engenharia, Universidade de São Paulo, São Carlos, Brasil, 204 p.

BORSARI RD. 1986. A cavitação do Escoamento sobre Vertedores em Degraus via CFD. Tese de Doutorado, Escola de Engenharia, Universidade de São Paulo, São Carlos, Brasil, 246 p.

CARVALHO PD. 1997. Aeração de Escoamentos de Alta Velocidade em Canais de Forte Declividade. Tese de Doutorado, Escola de Engenharia, Universidade de São Paulo, São Carlos, Brasil, 387 p.

CFX. 2004. CFX 5 Solver Theory. Ansys Canada Ltda, Waterloo, Ontario, Canada, 250 p.

CHANSON H. 1991. Aeration of a Free Jet Above a Spillway. J Hydraul Res 29(5): 655–667.

ERVINE DA, FALVEY HT AND KAHN AR. 1995. Turbulent Flow Structure and Air Uptake at Aerators. Hydropower and Dams, September, 89–96.

FUENTES R. 1992. Modelación Física en Hidráulica (Physical Modeling in Hydraulics), Actas del curso précongreso del XV Congreso Latinoamericano de Hidraulica, IAHR, Universidad de Cartagena, Colômbia.

KÖKPINAR MA AND GÖGÜS M. 2002. High-speed Jet Flows Over Spillway Aerators. Can J Civ Eng 29: 885–898.

BED AERATION IN SMOOTH CHANNELS: EXPERIMENTS AND NUMERICAL SIMULATION

LIMA ACM, SCHULZ HE AND GULLIVER JS. 2008. Air uptake in the lower nappe of a spillway aer
Hydraulic Res 46(6): 839–843. doi:10.3826/jhr.2008.3296.

LOW HS. 1986. Model Studies of Clyde Dam Spillway Aerators. Master Report, Ref 86-6, University of Cant
New Zealand.

PAN S, SHAO Y, SHI Q AND DONG X. 1980. The Self-aeration Capacity of the Water Jet Over the Aeration
J Hydr Engrg (Shuili Xuebao – in Chinese with abstract in English), Beijing, PRC, 5, Oct, 13–22.

PINTO NL DE S, NEIDERT SH AND OTA JJ. 1982. Aeration at High Velocity Flows. Water Power and Dam
34-38: 42–44.

RUTSCHMANN P AND HAGER WH. 1990. Air Entrainment by Spillway Aerators. J Hydr Engrg 116(6): 76

SCHWARZ I AND NUTT LP. 1963. Projected Nappes subjected to Transverse Pressure. J Hydr Div ASCE
97–104.

TAN P. 1984. Model Studies of Aerators and Spillways. Research Report 84-6, Dept Civil Engg,Univ of Cant
Christchurch, New Zealand.

TOOMBES L AND CHANSON H. 2005. Air Entrainment and Velocity Redistribution in a Bottom Outlet Je
XXXI IAHR Congress, September 11 to 16, Seoul, Korea, 2716–2726.

VOLKART P. 1980. The Mechanism of Air Bubble Entrainment in Self-Aerated Flow. Int Jf Multiphase F
411–423.

WILHELMS SC AND GULLIVER JS. 2005. Bubbles and Waves Description of Self-aerated Spillway Flow. J H
Res 43(5): 522–531.

WOOD IR. 1985. Air Water Flows, Keynote address, Proceedings of the 21th IAHR Congress, Melbourne, Au
6: 18–29.